Available online at www.sciencedirect.com

ScienceDirect

journal homepage: www.elsevier.com/locate/he

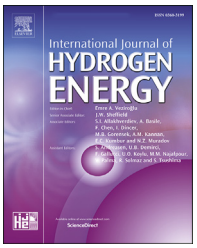

Moisture migration in the cathode GDL of PEMFC under variable physical parameters based on a modified two-fluid model

Minghui Zhang, Minjie Yu, Zhichun Liu, Zhengkai Tu[**], *Wei Liu*[*]

School of Energy and Power Engineering, Huazhong University of Science and Technology, Wuhan 430074, China

HIGHLIGHTS

- A modified two-fluid model with the momentum equations for gas and liquid is proposed.
- An algorithm for the liquid momentum equation is presented in place of Darcy's law.
- The velocity distribution of gas and liquid water for a single-unit cell is predicted.
- The effect of porosity on electrical performance and water migration is investigated.
- Optimal permeability is gained to ensure a low liquid saturation and high performance.

ARTICLE INFO

Article history:
Received 17 November 2022
Received in revised form
25 December 2022
Accepted 5 January 2023
Available online xxx

Keywords:
Proton exchange membrane fuel cell
Two-fluid model
Distribution and transport of moisture
Gas diffusion layer

ABSTRACT

To predict the morphology and migration of water in the porous electrode of proton exchange membrane fuel cell (PEMFC) more accurately, a modified mathematical model of with extensions of the original two-fluid model is presented based on the heat and mass transfer model of unsaturated porous media. The model integrated the mechanisms of the capillary effect, pressure, diffusion, and phase-to-phase interaction, and was applied to the numerical study of the single-fluid channel cell herein. The results show that the interaction between the gas and liquid is dominated by the drag force caused by relative motion, which highly depends on the position and local water saturation. What's more, a higher porosity facilitates the discharge of liquid and gaseous water in the GDL, while for the permeability, there exists a local optimum value which leads to a lowest liquid saturation in the GDL and helps to avoid the flooding phenomenon.

Introduction

Among the common chemical energy conversion and utilization devices, fuel cell (FC) has been receiving more and more attention for their high efficiency, low pollution and low noise [1]. The proton exchange membrane fuel cell (PEMFC) is more suitable for various portable power equipment and distributed power generation systems because of its lower operating temperature and faster start-stop response than other types of fuel cells [2].

The main operating principle of PEMFC is shown in Fig. 1. At the anode, hydrogen is transported through the flow channel and gas diffusion layer (GDL) to the catalyst layer (CL) where the reduction reaction of hydrogen occurs to generate

* *Corresponding author.*
** *Corresponding author.*
E-mail addresses: tzklq@hust.edu.cn (Z. Tu), w_liu@hust.edu.cn (W. Liu).

https://doi.org/10.1016/j.ijhydene.2023.01.055

Nomenclature

a	water activity
C	mole concentration, $mol \cdot m^{-3}$
C_p	specific heat at constant pressure, $J \cdot kg^{-1} \cdot K^{-1}$
D	diffusion coefficient, $m^2 \cdot s^{-1}$
EW	equivalent weight of the membrane, $kg \cdot mol^{-1}$
F	faraday constant, $C \cdot mol^{-1}$
J	exchange current density, $A \cdot m^{-1}$
$J(s)$	Leverett-J function
K	absolute permeability, m^2
k_r	relative permeability, m^2
k	thermal conductivity, $W \cdot m^{-2} \cdot K^{-1}$
L_h	latent heat, $W \cdot m^{-2}$
M	molecular weight, $mol \cdot kg^{-1}$
m	net evaporation of water, $kg \cdot m^{-3} \cdot s^{-1}$
n_d	electro-osmotic drag coefficient
p	pressure, Pa
R	universal gas constant, $J \cdot mol^{-1} \cdot K^{-1}$
S	source term
ΔS	entropy change in electrochemical reactions, $J \cdot mol^{-1} \cdot K^{-1}$
s	water saturation
T	temperature, K
u, v, w	the velocity component in the x, y and z directions, $m \cdot s^{-1}$
$\vec{V}$	velocity, $m \cdot s^{-1}$
v	volume, m^3
X	molecular fraction
Y	mass fraction

Greek symbols

γ	evaporation and condensation coefficients
δ	dimensionless correction factor of Darcy's function
ε	porosity
η	over potential of half cell, V
θ_c	contact angle, °
κ	electric conductivity, S
λ	dissolved water content
μ	coefficient of dynamic viscosity, $Pa \cdot s$
ξ	stoichiometric ratio
ρ	density, $kg \cdot m^{-3}$
σ	the tension coefficient of water, $N \cdot m^{-1}$
φ	electric potential, V
ϕ	a specific physical field variable

Subscripts

a	anode
c	cathode
ch	channel
$cond$	condensation
d	dissolved phase
D	the state corresponding to the reference value D^0
e	electron
eq	equilibrium
$evap$	evaporation
g	gas phase
i	a specific gas component
l	liquid phase
m	proton exchange membrane
r	relative
sat	saturated
v	vapor

Superscripts

eff	effective
ref	reference
0	original value

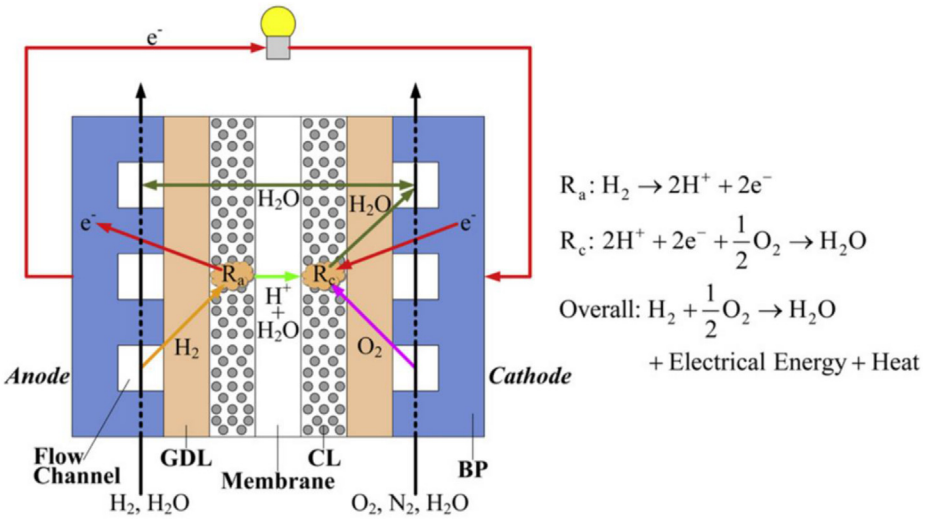

Fig. 1 – Schematic of the operating principle of PEMFC [4].

Please cite this article as: Zhang M et al., Moisture migration in the cathode GDL of PEMFC under variable physical parameters based on a modified two-fluid model, International Journal of Hydrogen Energy, https://doi.org/10.1016/j.ijhydene.2023.01.055

protons and electrons. Due to the selective permeability of the proton exchange membrane, protons are selectively transported across the membrane to the cathode, while electrons are transported to the cathode via an external circuit. Similarly, oxygen is transported to the CL via the flow channel and GDL on the cathode side, where it combines with protons and electrons in an oxidation reaction to produce water and emit heat. For PEMFC, the typical operating temperature is in the range of 40–90 °C [3]. Therefore, both vapor and liquid water will be present inside the cell. On the one hand, the ion transport capacity of the PEMFC relies on its own wettability, which requires the cell interior not to be excessively dry; on the other hand, too much liquid water in the GDL and CL will block the pores and hinder the transport of the reacting gas to the electrochemical reaction sites. A good understanding of the heat and mass transfer mechanisms inside the cell, especially in the GDL, is fundamental and critical for achieving the excellent transport and distribution of moisture and heat in the PEMFC.

Currently, the research on the heat and mass transfer mechanism of GDL mainly relies on two means: experimental tests and numerical modeling. With the help of experimental tests, researchers can directly observe various heat and mass transfer phenomena in each component of the cell or even the whole cell, and obtain the effects of different materials and processes on the cell performance [5–7], which is helpful to understand the material properties and energy mass transfer characteristics in the cell [8]. However, numerous physical field variables are involved in PEMFC, such as gas components and water saturation. The observation and quantitative analysis of the in-situ spatial distribution of these physical quantities remain a difficult task in experimental testing. Compared with experimental tests, numerical simulations can provide quantitative estimation of the distribution of physical fields by introducing certain assumptions, which have the characteristics of short time, low cost and good generalization, and have become an important tool for scholars worldwide to study the transport mechanism of PEMFC.

The numerical modeling of PEMFC, which involves the mechanisms of basic flow, porous media, transmembrane transport and electrochemical, has been extensively studied and developed over the past three decades, covering macroscopic, mesoscopic and microscopic scales [9]. Springer et al. [10] and Bernardi et al. [11] were the first to propose a one-dimensional isothermal model of PEMFC and investigated the effect of membrane water content on the membrane performance, and the effect of the distribution of each physical field within the cell on the cell performance, respectively. To further understand the mass transfer characteristics in different directions, various quasi-two-dimensional [12,13] and two-dimensional models [14,15] have been gradually developed, in which some non-isothermal models have also emerged for investigating the hydrothermal management of the cell. With the improvement of computing power, three-dimensional models were fully developed. Berning et al. [16,17] modeled a single flow channel in three dimensions based on a two-fluid model, estimated the distribution of each physical field in the porous media layer of the cell cathode by simplifying the momentum conservation equation of gas and liquid to Darcy's equation, and described the mechanisms of gas and liquid transport. Since then, Meng et al. [18], Adroher et al. [19], Havaej et al. [20], and Zhang et al. [21] coupled more models on the two-fluid model of Berning et al. for studying various transport phenomena within the cell. The three-dimensional models of PEMFC created by Wang et al. [22] based on the mixed fluid model have also been followed by many researchers [23–25]. In recent years, a number of researchers have also conducted targeted studies on membrane electrode components of cells at mesoscopic [26] and microscopic [27] scales, and the internal transport mechanism of cells has been more clearly understood.

With the continuous development of the PEMFC model, the fuel cell model has become increasingly sophisticated and complex. Due to the difficulty of mesoscopic and microscopic scale models to comprehensively describe the various mechanisms, macroscopic modeling plays an important role in guiding the design and production of PEMFC. And the accuracy and applicability of the model determine the credibility of the calculation results, and further determine the capacity of the model to predict the problems that may occur in the operation of the cell. Among the macroscopic models currently applied to porous media, the mainstream models are mainly the multiphase mixture model and the two-fluid model. For the former, the gas and liquid need to be treated as a hypothetical single-phase fluid [28], which ignores the interaction between the two phases and cannot accurately predict the moisture migration as vapor and liquid water in porous media. As for the latter, the governing equations for the gas and liquid phases are solved separately, and the momentum equation for liquid water is mostly downgraded to the form of Darcy's equation to simplify the solution. Even if the correction of relative permeability is applied to improve the calculation accuracy, this model still cannot consider well the interaction between gas, solid and liquid phases in porous media, as well as the effect of the phase change between the liquid water and vapor.

In this paper, a macroscopic, three-dimensional, non-isothermal, unsaturated two-phase flow heat and mass transfer model and an accompanying iterative algorithm were proposed based on the unsaturated (considered as gas and liquid coexistence in porous media) porous media model summarized in previous researches [29]. The model complemented the calculation method of vapor velocity, and considered the interactions between the gas, liquid and solid phases in the porous media by replacing the Darcy equation with the liquid water conservation equation. Herein, this model was applied to the diffusion layer of the cathode to analyze the distribution and transport of moisture for the single-unit cell, and the model was compared with the commonly used two-fluid model. The effects of different cathode GDL with variable porosity and permeability on the moisture migration and the cell electrical performance were also investigated, thus providing guidelines for subsequent researches on variable parameters and structural improvement.

Please cite this article as: Zhang M et al., Moisture migration in the cathode GDL of PEMFC under variable physical parameters based on a modified two-fluid model, International Journal of Hydrogen Energy, https://doi.org/10.1016/j.ijhydene.2023.01.055

Model development

Assumption

In order to apply the mathematic model in this paper for calculation, the following assumptions need to be satisfied.

(1) The PEMFC is operating under steady state.
(2) All flows in the PEMFC are considered as laminar flows due to the very slow fluid velocities.
(3) The gravity is neglected.
(4) The porous media material is homogeneous, that is, the physical properties are the same for any representative elemental volume.
(5) The flows of gas and liquid phases in the porous media satisfy continuity.
(6) The gas mixture is considered as an ideal gas.

It should be mentioned that the anisotropy of porous media materials has been investigated by some researchers [30]. However, the effect of that is not within the scope of this study. Thus, the assumption of homogeneity is still chosen for this study to simplify the calculation procedure.

In addition, considering the coexistence of gas and liquid phase flow in the porous media of the cell, which is also called unsaturated two-phase flow, both phases can be assumed to be continuous and a macroscopic mathematical model can be constructed based on the REV assumption. A random computational domain unit in a porous media is shown in Fig. 2, where the dark part is the solid skeleton, the light part is the liquid-phase fluid, and the blank part is the gas-phase fluid. According to the assumption of continuity, it is considered that in porous media, the liquid flows as a liquid film attached to the surface of the solid skeleton, while the gas exists between the liquid films in the porous media, especially in the larger pores. Thus, the continuity assumptions are satisfied for the solid, liquid, and gas phases in porous media, respectively. What's more, the physical field variables of a specific REV depend on the weighted average of the variables for its internal phases [32], as shown follows:

$$\langle\phi\rangle = \frac{1}{v}\int_{v}\phi \mathrm{d}v \tag{1}$$

where ϕ is any physical field variable, such as temperature and water saturation, $\langle\phi\rangle$ is the volume-averaged physical field variable, and v is the volume of the selected REV. If a specific variable is exclusive to a phase, such as the velocity of the liquid phase $\vec{V_l}$, the value of it is considered as 0 for the other phases. We obtain the equation of each physical field variable with respect to the coordinate position based on the above volume averaged method, so that numerical calculations can be carried out conveniently with the methods of common computational fluid dynamics. In order to simplify the expression of the equation, all variables to be solved in this paper are volume averaged so that they are no longer extra identified with the symbol $\langle\phi\rangle$.

Governing equations

In previous studies, the two-fluid model has been shown to be a more comprehensive model than others for describing the two-phase flow behavior in PEMFC. However, most researchers reduce the liquid water momentum equation to Darcy's function to simplify the calculation, which may bring about large errors and cannot fully predict the phenomena of moisture migration. In the present study, an unsaturated two-fluid model was applied in cathode GDL for the first time to obtain the real transport velocity distribution of liquid water and vapor. And the model mentioned above will be described in detail in subsection 2.2.2 and compared with the original two-fluid model.

Model of gas transport

In PEMFC, the transport processes of the gas in the flow channel, GDL and CL are described by the continuity equation and the momentum conservation equation. In order to consider the diffusion effect between the components of the gas, the component conservation equation is introduced to calculate the concentration of each component [4].

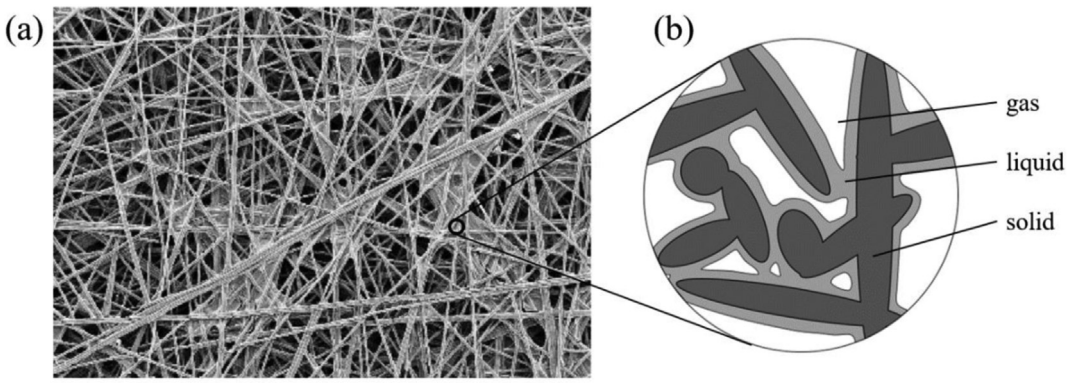

Fig. 2 – Schematic of the morphology and the internal component composition of GDL: (a) SEM image of GDL [31] and (b) representative elementary volume.

Please cite this article as: Zhang M et al., Moisture migration in the cathode GDL of PEMFC under variable physical parameters based on a modified two-fluid model, International Journal of Hydrogen Energy, https://doi.org/10.1016/j.ijhydene.2023.01.055

Table 1 – Source terms.

Source term	Unit
$S_{gm} = \begin{cases} \dot{m} + (1-s)\gamma_{dv}\rho_m(\lambda-\lambda_{eq})/EW + S_{H_2} & \text{(Anode CL)} \\ \dot{m} + (1-s)\gamma_{dv}\rho_m(\lambda-\lambda_{eq})/EW + S_{O_2} & \text{(Cathode CL)} \\ \dot{m} & \text{(GDLs, channel)} \end{cases}$	$kg\cdot m^{-3}\cdot s^{-1}$
$S_{gu} = -\frac{\mu_g}{Kk_{rg}}\frac{(1-s)}{s}\left(\frac{\overrightarrow{V_g}}{\varepsilon s} - \frac{\overrightarrow{V_l}}{\varepsilon(1-s)}\right) + \dot{m}\frac{\overrightarrow{V_v}}{\varepsilon^2(1-s)^2}$ (Cathode GDL)	$kg\cdot m^{-2}\cdot s^{-2}$
$S_{H_2} = -\frac{M_{H_2}J_a}{2F}$ (Anode CL)	$kg\cdot m^{-3}\cdot s^{-1}$
$S_{O_2} = -\frac{M_{O_2}J_c}{4F}$ (Cathode CL)	$kg\cdot m^{-3}\cdot s^{-1}$
$S_{H_2O} = \begin{cases} \dot{m} + (1-s)\gamma_{dv}\rho_m(\lambda-\lambda_{eq})M_{H_2O}/EW & \text{(CLs)} \\ \dot{m} & \text{(GDLs, channel)} \end{cases}$	$kg\cdot m^{-3}\cdot s^{-1}$
$S_{lm} = \begin{cases} -\dot{m} + s\gamma_{dl}\rho_m(\lambda-\lambda_{eq})M_{H_2O}/EW & \text{(CLs)} \\ -\dot{m} & \text{(GDLs, channel)} \end{cases}$	$kg\cdot m^{-3}\cdot s^{-1}$
$S_{lu} = -\frac{\mu_l}{Kk_{rl}}\frac{\overrightarrow{V_l}}{\varepsilon s} + \frac{\mu_g}{Kk_{rg}}\frac{(1-s)}{s}\left(\frac{\overrightarrow{V_g}}{\varepsilon s} - \frac{\overrightarrow{V_l}}{\varepsilon(1-s)}\right) - \dot{m}\frac{\overrightarrow{V_l}}{\varepsilon^2 s^2}$ (Cathode GDL)	$kg\cdot m^{-2}\cdot s^{-2}$
$S_{mw} = \frac{J_c}{2F} - [(1-s)\gamma_{dv} + s\gamma_{dl}]\rho_m(\lambda-\lambda_{eq})/EW$ (CLs)	$mol\cdot m^{-3}\cdot s^{-1}$
$S_e = \begin{cases} -J_a & \text{(Anode CL)} \\ J_c & \text{(Cathode CL)} \end{cases}$	$A\cdot m^{-3}$
$S_{ion} = -S_e$	$A\cdot m^{-3}$
$S_T = \begin{cases} J_a\left(\lvert\eta_a\rvert + \frac{T\Delta S_a}{2F}\right) + \kappa_e^{eff}\lVert\nabla\varphi_e\rVert^2 + \kappa_{ion}^{eff}\lVert\nabla\varphi_{ion}\rVert^2 + S_{lm}L_h & \text{(Anode CL)} \\ J_c\left(\lvert\eta_c\rvert + \frac{T\Delta S_c}{4F}\right) + \kappa_e^{eff}\lVert\nabla\varphi_e\rVert^2 + \kappa_{ion}^{eff}\lVert\nabla\varphi_{ion}\rVert^2 + S_{lm}L_h & \text{(Cathode CL)} \\ \kappa_e^{eff}\lVert\nabla\varphi_e\rVert^2 + S_{lm}L_h & \text{(GDLs)} \\ \kappa_{ion}^{eff}\lVert\nabla\varphi_{ion}\rVert^2 & \text{(membrane)} \end{cases}$	$W\cdot m^{-3}$

$$\nabla\cdot\left(\rho_g\overrightarrow{V_g}\right) = S_{gm} \tag{2}$$

$$\nabla\cdot\left(\frac{\rho_g\overrightarrow{V_g}\overrightarrow{V_g}}{\varepsilon^2(1-s)^2}\right) = -\nabla p_g + \nabla\cdot\left(\mu_g\nabla\left(\frac{\overrightarrow{V_g}}{\varepsilon(1-s)}\right)\right) + S_{gu} \tag{3}$$

$$\nabla\cdot\left(\rho_g\overrightarrow{V_g}Y_i\right) = \nabla\cdot\left(\rho_g D_i^{eff}\nabla Y_i\right) + S_i \tag{4}$$

The source terms of the governing equations are listed in Table 1 to ensure the simplicity of the equations. For the gas transport model, the source terms associated with the phase transition are added to the three equations above; in addition, since the flow region of the gas is encapsulated by a liquid film, liquid drag resistance is introduced to describe the drag force between the liquid phase and the gas phase.

Since the microstructure of porous media is neglected in this calculation, the effective diffusion coefficient in porous media needs to be calculated with the Bruggeman's correction on the basis of the ordinary diffusion coefficient. See Table 2 for the equations of physical parameters and Table 3 for operating and geometric parameters.

Water vapor is the prime part of moisture in porous media. The direction of its migration depends mainly on the overall flow of the gas, as well as on the diffusion caused by the concentration gradient. Thus, the transport velocity of water vapor can be calculated by the Fick's law and the definition equation of gas diffusion:

$$\overrightarrow{V_{v,d}} = -D_i^{eff}\nabla Y_i \tag{5}$$

$$\overrightarrow{V_v} = \overrightarrow{V_g} + \overrightarrow{V_{v,d}} \tag{6}$$

where $\overrightarrow{V_{v,d}}$ is the diffusion velocity of the vapor, and $\overrightarrow{V_v}$ is the absolute migration velocity of the vapor, which can be expressed mathematically as a vector sum of the gas velocity and the diffusion velocity in the form [29,33].

Model of liquid transport

For PEMFC working below the boiling point of water, liquid water usually coexists with water vapor internally. In GDL, the presence of liquid water may block the pores inside the porous media and thus impede the transport of the reactant gas to the reaction sites. In fact, due to the diverse and rather complex internal structure of porous materials, it is too idealistic to adopt the assumption of homogeneity in the numerical simulations, which may result in an excessive prediction of the PEMFC performance compared with the actual process. Therefore, in addition to the electrochemical performance, the liquid water distribution in the PEMFC should also receive focused attention, which can help to predict the location of localized blockages in the GDL and take measures to avoid the phenomenon as much as possible.

Numerous researchers have used two-fluid model to obtain the distribution of liquid water in porous media. In this model, the saturation and transport velocity of the liquid are usually calculated using the continuity equation of the liquid and Darcy's equation, as shown follows:

$$\nabla\cdot\left(\rho_l\overrightarrow{V_l}\right) = S_{lm} \tag{7}$$

Please cite this article as: Zhang M et al., Moisture migration in the cathode GDL of PEMFC under variable physical parameters based on a modified two-fluid model, International Journal of Hydrogen Energy, https://doi.org/10.1016/j.ijhydene.2023.01.055

Table 2 – Physical parameters.

Parameter	Expression
relative permeability, -	$k_{rg} = (1-s)^{4.0}$ $k_{rl} = s^{4.0}$
effective diffusion coefficient, $m^2 \cdot s^{-1}$	$D_i^{eff} = \varepsilon^{1.5}(1-s)^{1.5}\left(\frac{p_D^{ref}}{p}\right)\left(\frac{T}{T_D^{ref}}\right)^{1.5} D_i^0$
saturation pressure, Pa	$\log_{10}(p_{sat}/101325) = -2.1794 + 2.953\times10^{-2}(T-273.15) - 9.1837\times10^{-5}(T-273.15)^2 + 1.4454\times10^{-7}(T-273.15)^3$
EOD coefficient, -	$n_d = \frac{2.5\lambda}{22}$
equilibrium water content, -	$\lambda_{eq} = \begin{cases} 0.043 + 17.81a - 39.85a^2 + 36.0a^3 & 0 \le a \le 1 \\ 14.0 + 1.4(a-1.0) & 1 < a \le 3 \end{cases}$
water activity, -	$a = \frac{p_v}{p_{sat}} + 2s$
dissolved water diffusion coefficient, $m^2 \cdot s^{-1}$	$D_d^{eff} = \begin{cases} 3.1\times10^{-3}\lambda(\exp(0.28\lambda)-1)\exp(-2346/T) & (0<\lambda\le3) \\ 4.17\times10^{-8}\lambda(1+161\exp(-\lambda))\exp(-2346/T) & (\lambda>3) \end{cases}$
proton conductivity, $S \cdot m^{-1}$	$\kappa_{ion} = (0.514\lambda - 0.326)\exp[1268(1/303 - 1/T)]$
electron conductivity, $S \cdot m^{-1}$	$\kappa_e^{eff} = \kappa_e^0(1-\varphi)^{1.5}$
exchange current density, $A \cdot m^{-3}$	$J_a^{ref} = 10^8 \exp\left(-1400\left(\frac{1}{T} - \frac{1}{353.15}\right)\right)$ $J_c^{ref} = 120 \exp\left(-7900\left(\frac{1}{T} - \frac{1}{353.15}\right)\right)$

$$\vec{V_l} = -\frac{Kk_{rl}}{\mu_l}\nabla p_l \tag{8}$$

after eliminating the velocity of liquid water, the above equation can be expressed as:

$$\nabla \cdot \left(\rho_l \frac{Kk_{rl}}{\mu_l}\nabla p_l\right) + S_{lm} = 0 \tag{9}$$

Eq. (9) is the common liquid water transport equation, which has been widely used in various numerical calculations using the two-fluid model. However, the model is derived based on Darcy's law, which requires that the flow in the porous media is saturated (single-phase) and the relative permeability is introduced to ensure that Darcy's formula can also be solved relatively correctly in two-phase calculations. The relative permeability of the gas and liquid phases can be derived from empirical formulas, as shown in Table 2.

Table 3 – Operating and geometric parameters.

Parameter	Value
channel length, mm	70.0
channel width, mm	1.0
channel height, mm	1.0
membrane width, mm	2.0
thickness (GDL, CL, membrane), mm	0.3, 0.0129, 0.108
porosity (CL)	0.25
absulote permeability (CL), mm	$1.0e^{-14}$
contact angle (GDL, CL), °	120, 100
density of dry membrane, $kg \cdot m^{-3}$	1980
equivalent weight of membrane, $kg \cdot mol^{-1}$	1.1
operation temperature, K	343.15
operation pressure (Anode, Cathode), atm	3.0, 3.0
stoichiometric ratio (H_2, O_2)	2.0, 1.5
relative humidity of inlet gas (Anode, Cathode)	100%, 100%
reference current density, $A \cdot m^{-3}$	16,000
reference concentration (H2, O2), $mol \cdot m^{-3}$	56.4, 3.39
liquid water density, $kg \cdot m^{-3}$	977.85
viscosity coefficient of liquid water, $N \cdot s \cdot m^{-2}$	$4.05e^{-4}$
surface tension coefficient, $N \cdot m^{-1}$	0.0625
latent heat of water condensation, $J \cdot kg^{-1}$	2,263,073
phase change coefficient of water, s^{-1}	100
phase change coefficient of dissolved water (gas, liquid), s^{-1}	1.0, 1.0

It should be noted that even if the relative permeability correction is used, it is still difficult to guarantee a high accuracy of the results because Darcy's law only considers the dragging effect of the solid skeleton on the flow, while ignoring its own inertia and the interaction between multiple phases. In serpentine flow channels and other more complex flow channels, correction terms need to be introduced to obtain more accurate results. Chen et al. [34] used the Forchheimer's correction to consider the effect of inertia on liquid transport. It is easy to see that with the increasingly complex design of PEMFC flow channels and porous material structures, a single Darcy's law cannot satisfy the computational requirements. To investigate the two-phase flow behavior occurring inside porous materials by solving the macroscopic equations, the interaction between the two phases, as well as the ubiquitous phase transition, must be taken into account.

To solve these problems, the Darcy equation (Eq. (8)) from the previous model is replaced by the momentum equation for the liquid phase in the unsaturated porous media model, as shown in Eq. (10) [29,32,33].

$$\nabla \cdot \left(\frac{\rho_l \vec{V_l}\vec{V_l}}{\varepsilon^2 s^2}\right) = -\nabla p_l + \nabla \cdot \left(\mu_l \nabla\left(\frac{\vec{V_l}}{\varepsilon s}\right)\right) + S_{lu} \tag{10}$$

This equation for the liquid phase shows the same form as the momentum equation for the gas phase: the left side of the equation represents the convective effect of the liquid phase, the first term on the right side represents the driving effect of the liquid phase pressure gradient on the liquid, the second term represents the viscous diffusion effect within the liquid, and the third term is the source term, in which all interactions

Please cite this article as: Zhang M et al., Moisture migration in the cathode GDL of PEMFC under variable physical parameters based on a modified two-fluid model, International Journal of Hydrogen Energy, https://doi.org/10.1016/j.ijhydene.2023.01.055

and phase change effects are involved. As can be seen from Table 1, the source term of the liquid phase momentum equation consists of three parts. The first part is the interaction between the liquid phase and the solid skeleton. Due to the assumption that the liquid phase is attached to the surface of the skeleton, the transport of the liquid will be affected by the surface force of the solid. And the closer the liquid to the surface of the skeleton, the more difficult it is to migrate. The second part reflects the interaction between the liquid and gas phases, where the liquid is least bound by the solid skeleton at the interface between the gas and liquid phases, and thus the flow is most likely to occur. The relative velocity between the gas and liquid produces a mutual dragging effect, which leads to an exchange of momentum between the two phases, so this part will also be reflected in the source term of the gas-phase momentum equation. The third part reflects the contribution of the increase in mass caused by the phase change to the momentum change.

To simplify the solution of the liquid-phase momentum equation, the Leverett-J function is introduced to describe the empirical relationship between water saturation and capillary pressure [4]:

$$p_l = p_g - p_c \tag{11}$$

$$p_c = \sigma \cos\theta_c \sqrt{\frac{\varepsilon}{K}} J(s) \tag{12}$$

$$J(s) = \begin{cases} 1.42(1-s) - 2.12(1-s)^2 + 1.26(1-s)^3 & \theta_c < 90^\circ \\ 1.42s - 2.12s^2 + 1.26s^3 & \theta_c \geq 90^\circ \end{cases} \tag{13}$$

By applying the above equations to the calculation of Eqs. (7) and (10), the transport model of liquid water can be simplified to a set of equations about water saturation and liquid phase migration velocity. Thus, a more informative result can be obtained, which simultaneously considers four kinds of effects including capillary forces of porous media, Darcy's resistance of solid phase skeleton to liquid, the interaction at gas-liquid surfaces, and inertia forces of the liquid phase for transport.

Model of phase transition

For a conventional PEMFC (as opposed to a high-temperature PEMFC), phase changes occur in the flow channel and in the porous media because the operating temperature is below the boiling point of water. In this model, the widely adopted H-K-L equation, derived based on molecular dynamics, is used to calculate the evaporation/condensation source term, which can eventually be simplified to the following representation [4]:

$$\dot{m} = \begin{cases} \gamma_{cond}\varepsilon(1-s)\dfrac{p_{sat}-p_v}{RT} & p_v > p_{sat}(\text{condensation}) \\ \gamma_{evap}\varepsilon s\dfrac{p_{sat}-p_v}{RT} & p_v < p_{sat}(\text{evaporation}) \end{cases} \tag{14}$$

The H-K-L equation can be further organized and simplified to the following form [35]:

$$\dot{m} = \gamma_{lg}\varepsilon s\rho_g(X_{sat} - X_v) \tag{15}$$

where the coefficient γ_{lg} is referred to the parameter of the model in Ref. [35]. The calculated phase variables are added as source terms to the momentum conservation equation for gas and liquid, thus the influence of the phase change on the two-phase flow is taken into account.

Model of dissolved water transport

The membrane of PEMFC selectively allows the transport of protons across the membrane to the anode, and this mechanism works by relying on the SO_3^- groups on the membrane. Due to the hydrophilic properties of these groups, they absorb and combine with the surrounding water, achieving a wetted state. The water content is commonly used to describe the number of water molecules combined with each hydrophilic group and characterize the degree of wetting of a membrane. Because of the nature of the membrane itself, water molecules are transported across the membrane driven by electrochemical permeation and gradients, and the water content conservation equation of the membrane can be employed to describe this mechanism [4]:

$$\nabla\cdot\left(\frac{n_d}{F}\overrightarrow{j_{ion}}\right) = \nabla\cdot\left(\frac{\rho_m}{EW}D_d^{eff}\nabla\lambda\right) + S_{mw} \tag{16}$$

where the source term indicates the rate of generation and conversion of dissolved water. In the CL of PEMFC, the electrochemical reaction occurs at the three-phase interface between the membrane, the solid skeleton and the gas, and it can be assumed that the water produced by the cathode reaction exists in the form of dissolved water on the membrane. Since the ability of hydrophilic groups to bind water is limited, the equilibrium water content is introduced to describe the conversion of dissolved water. When the water content is less than the equilibrium water content, the free water near the membrane will tend to be bound to the membrane, and conversely, when the water content is greater than the equilibrium water content, the dissolved water of the membrane will be converted to free liquid or gaseous water. The calculation of the equilibrium water content relies on the empirical equations listed in Table 2 and the results are applied to the corresponding source terms in Table 1.

Model of electrochemical reaction

The electrochemical reaction model of PEMFC consists of charged particle generation and transport, obtained by solving two sets of coupled equations: the Butler-Volmer equations, which characterizes the chemical reaction rates, are calculated in CL, and the electron and proton conservation equations, which are used to calculate the direction and magnitude of current, are solved in CL, GDL (collector plates are not considered in this study), and membrane and CL, respectively. These equations can be expressed in the following form [36]:

$$J_a = J_a^{ref}\left(\frac{C_{H_2}}{C_{H_2}^{ref}}\right)^{0.5}\left(\exp\left(\frac{F\eta_a}{2RT}\right) - \exp\left(-\frac{F\eta_a}{2RT}\right)\right) \tag{17}$$

$$J_c = J_c^{ref}\left(\frac{C_{O_2}}{C_{O_2}^{ref}}\right)\left(-\exp\left(\frac{F\eta_c}{RT}\right) + \exp\left(-\frac{F\eta_c}{RT}\right)\right) \tag{18}$$

$$\nabla\cdot\left(\kappa_e^{eff}\nabla\varphi_e\right) + S_e = 0 \tag{19}$$

Please cite this article as: Zhang M et al., Moisture migration in the cathode GDL of PEMFC under variable physical parameters based on a modified two-fluid model, International Journal of Hydrogen Energy, https://doi.org/10.1016/j.ijhydene.2023.01.055

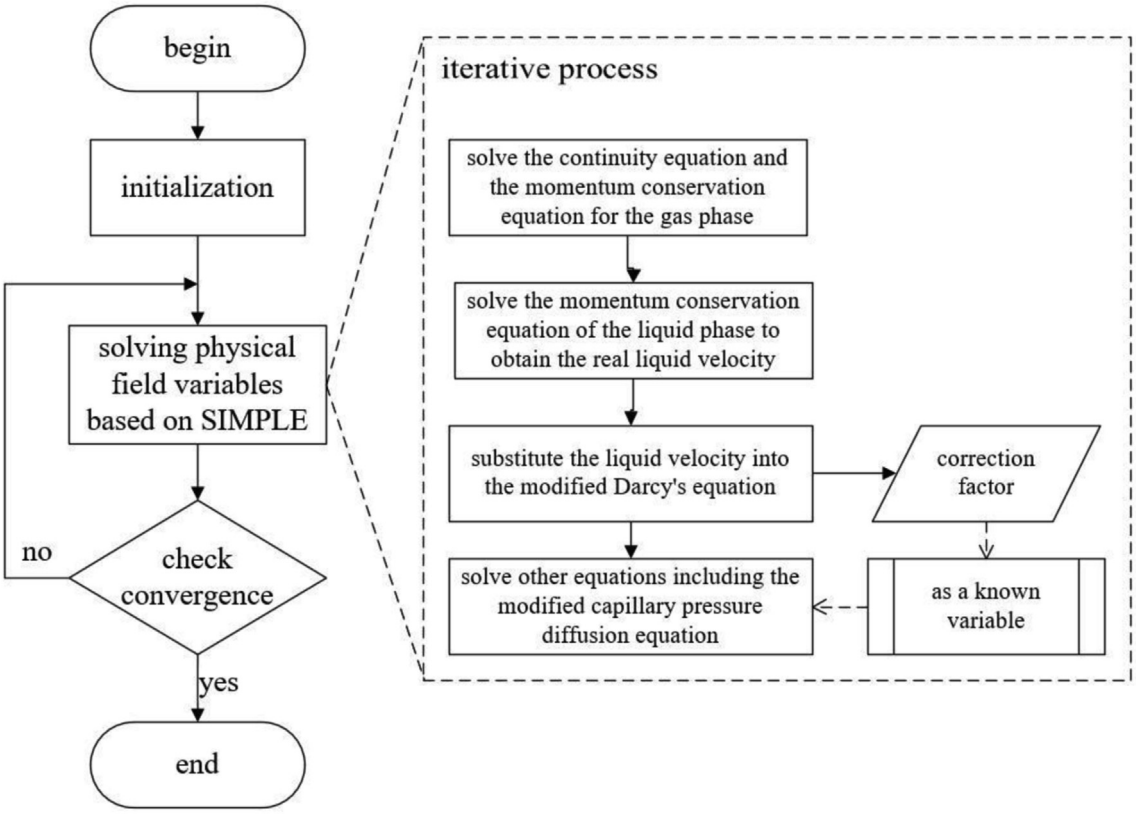

Fig. 3 – Iterative process for the modified two-fluid model.

$$\nabla \cdot \left(\kappa_{ion}^{eff} \nabla \varphi_{ion}\right) + S_{ion} = 0 \tag{20}$$

in these equations, the physical parameters are chosen with reference to the data in Table 3, and the contact resistance due to assembly is neglected in the solution.

Model of energy conservation

The cathode reaction of the PEMFC gives off heat, leading to a local temperature rise, which affects the migration behavior of the gases and liquids inside the cell. Hence the energy conservation equation is introduced, as shown in the following.

$$\nabla \cdot \left(\varepsilon s \rho_l C_{p,l} \vec{V_l} T + \varepsilon(1-s)\rho_g C_{p,g} \vec{V_g} T\right) = \nabla \cdot \left(k^{eff} \nabla T\right) + S_T \tag{21}$$

where k^{eff} is the effective thermal conductivity, which is calculated based on the weighted composition of the components of the characterized bulk element. The source term of the equation consists of four components: heat of polarization, heat of reaction, ohmic heat [37] and heat of phase change.

Numerical implementation

In the present study, all of the mathematical models introduced above are applied for predicting the physical fields of the PEMFC at steady state. It should be noted that the modified liquid transport model is only employed in the cathode GDL, because of the low level of liquid saturation in anode GDL. In fact, for this model, it is not easy to solve the liquid-phase continuity equation and the liquid-phase momentum equation (as known as Eqs. (7) and (10)) in a coupled manner, because Eq. (7) does not explicitly include the water saturation s as a variable, which is one of the reasons why derived capillary pressure diffusion equation based on the Darcy's law of the liquid phase are widely used. In order to enhance the convergence of the modified model, this paper combines the advantages of Darcy's law and proposes a matching improved algorithm based on the SIMPLE algorithm and capillary pressure diffusion equation, whose main solution ideas are shown in Fig. 3.

By replacing the Darcy equation with the momentum equation for liquid water, a modified capillary pressure diffusion equation in the shape of Eq. (9) was obtained, as follows:

$$\frac{\partial}{\partial x}\left(\rho_l \frac{K k_{rl}}{\mu_l(1+\delta_x)} \frac{\partial p_l}{\partial x}\right) + \frac{\partial}{\partial y}\left(\rho_l \frac{K k_{rl}}{\mu_l(1+\delta_y)} \frac{\partial p_l}{\partial y}\right) + \frac{\partial}{\partial z}\left(\rho_l \frac{K k_{rl}}{\mu_l(1+\delta_z)} \frac{\partial p_l}{\partial z}\right) + S_{lm} = 0 \tag{22}$$

where $\vec{\delta}$ is introduced as a dimensionless Darcy's law correction factor to describe the deviation of the liquid velocity obtained by solving the momentum equation for liquid water from the liquid velocity of Darcy's law prediction.

When the calculation results reach convergence, the residuals of the above equation also tend to stabilize, and a more accurate capillary pressure field can be obtained by Eq. (22) compared with that of Eq. (9), which means that a more informative water saturation distribution field can be obtained.

Please cite this article as: Zhang M et al., Moisture migration in the cathode GDL of PEMFC under variable physical parameters based on a modified two-fluid model, International Journal of Hydrogen Energy, https://doi.org/10.1016/j.ijhydene.2023.01.055

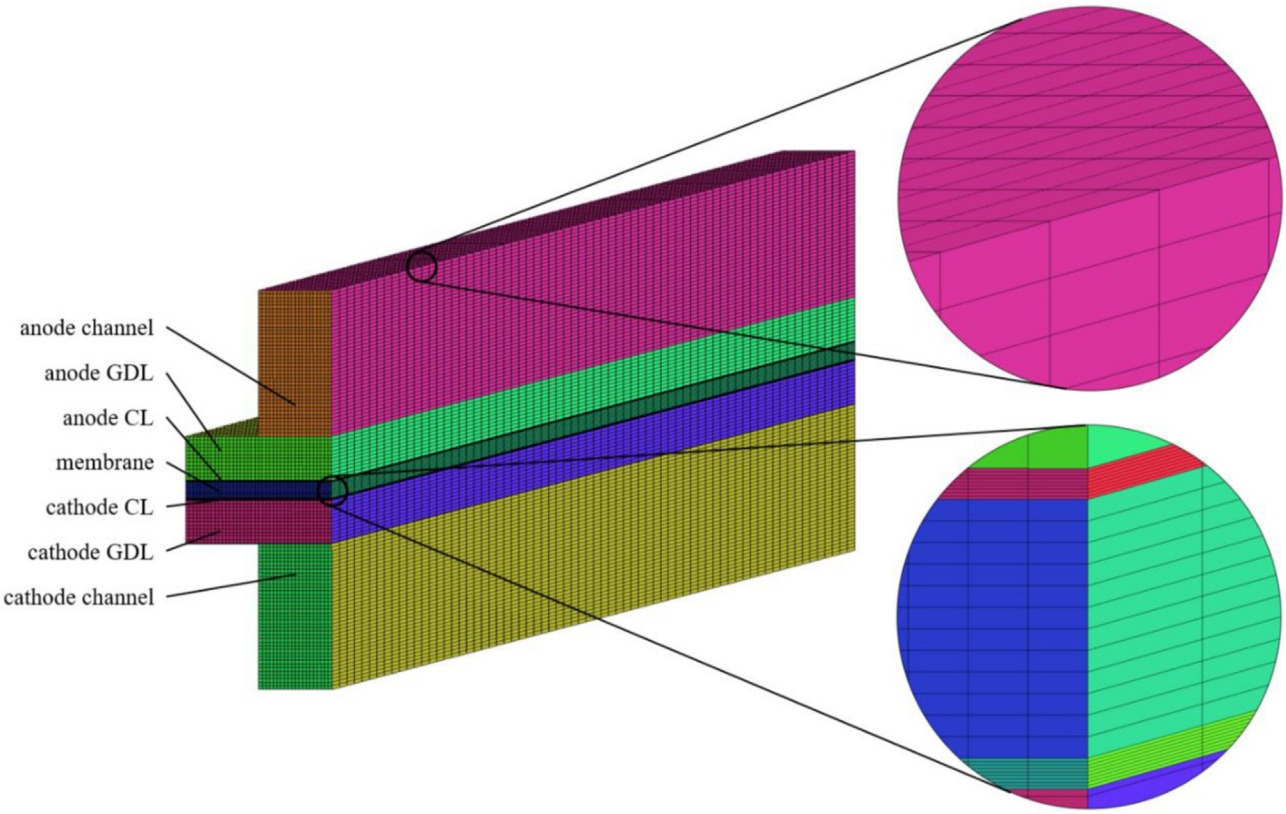

Fig. 4 – Schematic of computation domain and mesh of the single-channel PEMFC.

Model validation

Fig. 4 shows the geometric model and the mesh established for the PEMFC of a single flow channel with reference to the experiments of Wang et al. [36] In order to reduce the computational effort, the computational domain is reduced by half using symmetric boundary conditions, and the main geometric and physical parameters of the model are shown in Table 3. The flow rates of the cathode and anode inlets are obtained according to the following equation [21]:

$$m_a = \frac{\rho_g^a \xi^a I^{\mathrm{ref}} A_{act}^a}{2F C_{H_2} A_{inlet}^a} \tag{23}$$

$$m_c = \frac{\rho_g^c \xi^c I^{\mathrm{ref}} A_{act}^c}{4F C_{O_2} A_{inlet}^c} \tag{24}$$

$$C_{H_2} = \frac{p_{out}^a + \Delta p_{ch}^a - RH_a p_{sat}}{RT} \tag{25}$$

$$C_{O_2} = \frac{0.21\left(p_{out}^c + \Delta p_{ch}^c - RH_c p_{sat}\right)}{RT} \tag{26}$$

where the subscripts a and c represent the anode and cathode, respectively, ρ_g represents the gas density at the inlet, ξ represents the stoichiometric ratio, I^{ref} is the reference operating current density, A_{act} and A_{inlet} represent the reaction area and inlet area of the PEMFC, respectively, and RH represents the relative humidity of the reaction gas. The concentrations C_{H2} and C_{O2} of the reaction components at the inlet can be derived using Dalton's law of partial pressures, and the pressure drop Δp_{ch} along the flow channel can be approximated as 0 since the flow channel in this model is a single straight channel. All of the above parameters can be found in Table 3. The pressure-out condition with zero back pressure was applied at the exit of the flow channel. In addition, for the liquid in the cathode GDL, the slip-free boundary condition is used since the slip flow behavior at the wall is neglected due to the large viscosity. Since the modeling of the bipolar plate is neglected, the boundary condition of constant wall temperature is used for all walls in contact with the plate, while the others are set to adiabatic. The wall reference voltage at the anode in contact with the pole plate was set to 0 V, and the voltage at the cathode was set according to the specific operating conditions.

In order to ensure the credibility of the model, grid independence verification and model reliability verification are implemented. The grid independence verification results of the model are given in Table 4, and a partitioning scheme of 263,200 grids is selected. The computational results of this scheme are compared with the experimental data of Wang et al. [36], and the differences are shown in Fig. 5. In the validation process, the same operational parameters as the experiment are chosen. It can be seen that the model is consistent with the experimental results in terms of trend and the numerical error is relatively small, which means that the model has a high degree of confidence.

Please cite this article as: Zhang M et al., Moisture migration in the cathode GDL of PEMFC under variable physical parameters based on a modified two-fluid model, International Journal of Hydrogen Energy, https://doi.org/10.1016/j.ijhydene.2023.01.055

Table 4 – The numerical result at V_{cell} = 0.5 V for different grid systems.

grid systems	grid number			current density	relative difference	liquid saturation	relative difference
	x-axis	y-axis	z-axis				
136,192	32	108	56	1.5088	0.16%	0.0947	4.99%
263,200	40	134	70	1.5106	0.04%	0.0919	1.88%
417,312	46	154	84	1.5111	0.01%	0.0909	0.78%
532,350	50	167	91	1.5112	–	0.0902	–

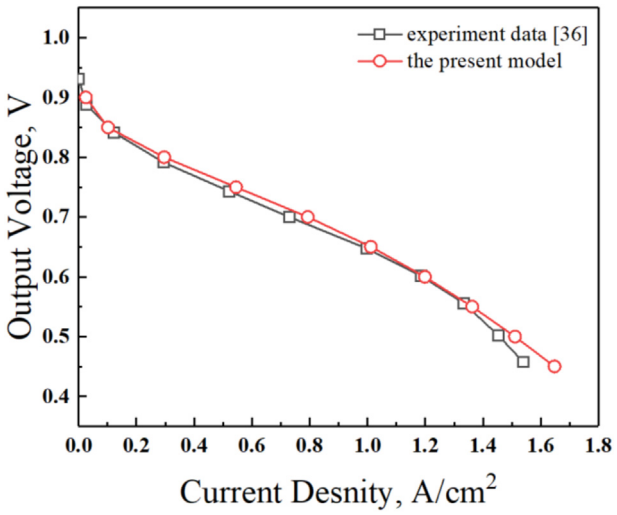

Fig. 5 – The comparisons of polarization curves of current model and experimental data.

Results and discussion

In this paper, the mathematical model introduced in the previous section is applied to obtain the distribution and migration of moisture in the cathode GDL, and a comparative analysis with the original Darcy's model was also carried out. In addition, by changing the macroscopic physical parameters of the cathode GDL, i.e., porosity and permeability, the moisture migration is obtained under different physical properties, and the effects on the electrical performance of the PEMFC were discussed.

Migration of water vapor

As one of the main components of the gas, the transport mechanism of water vapor in the cathode GDL has a very important influence on the mass transfer of oxygen. Since the gas satisfies continuity and is enveloped by a liquid film, a continuous gas pore channel is formed throughout almost the entire porous media. In this case, water vapor has different transport mechanisms inside the gas pore channel and at the gas-liquid interface. In the interior of the gas pore channel, the overall flow of gas driven by the pressure gradient affects the transport of water vapor, and the cathode reaction causes concentration and temperature differences in the PEMFC, which leads to the diffusive effect of water vapor. At the gas-liquid interface, the gas-liquid phase velocity difference and phase change can be the fundamental mechanisms affecting water vapor transport.

The distribution and migration of water vapor inside the cathode GDL at different output voltages are selected in Fig. 6. The porosity of the cathode GDL for this model is 0.4, the permeability is 1.76×10^{-11} m^2, and the three plots of (a) (b) (c) correspond to the results at an external voltage of 0.7 V, 0.6 V, 0.5 V, corresponding to the low, media and high current densities. Each plot gives pictures of the data at three locations along the flow direction in channel at 20%, 50% and 80% of the cell length. For the water vapor, the concentration gradient is the dominant driving force. As can be seen from the figure, the concentration of water vapor on the CL side (at the upper side) is higher than that on the channel side (at the lower side) due to the cathode chemical reaction, and it is lower on the channel side (at the middle side) than on the rib side (at the left and right sides). The distribution of water vapor determines the direction of diffusion. Driven by the concentration gradient, water vapor migrates from the CL side to the channel side and finally discharges into the channel. At the rib side of the GDL, the rib plate obstructs the normal transport of water vapor, and therefore the water vapor at the intersection of the channel and the GDL is squeezed more rapidly, especially in the region near the wall of the channel.

At a certain current density, the farther away from the cathode inlet, the higher the level of water vapor concentration in the GDL. There are two main factors contributing to this phenomenon: one is that the water vapor in the GDL can only be discharged to the channel, and the increase of the water vapor concentration in the channel will inhibit the diffusion of vapor from the GDL to the channel; the second is that the total pressure of the gas in the channel along the flow direction shows a tendency of decreasing, and the reduction of the pressure difference makes it more difficult to discharge the steam with the flow. According to the velocity trend of water vapor in the plot, it is also clearly to see that the discharge of water vapor along the flow direction in the flow channel is gradually weakened. For example, under the working conditions of 0.6 V, the average surface discharge velocity of the three surfaces are 9.793×10^{-3}, 6.541×10^{-3}, 4.844×10^{-3} m/s, respectively, which confirms the previous analysis.

As the current density increases, the migration rate of water vapor into the flow channel is enhanced. The main reason for this is that the overall water vapor content in the GDL increases as the cathode reaction rate and the concentration gradient increases, which leads to the diffusion of water vapor into the flow channel more significant. In addition, the higher water vapor concentration also leads to a

Please cite this article as: Zhang M et al., Moisture migration in the cathode GDL of PEMFC under variable physical parameters based on a modified two-fluid model, International Journal of Hydrogen Energy, https://doi.org/10.1016/j.ijhydene.2023.01.055

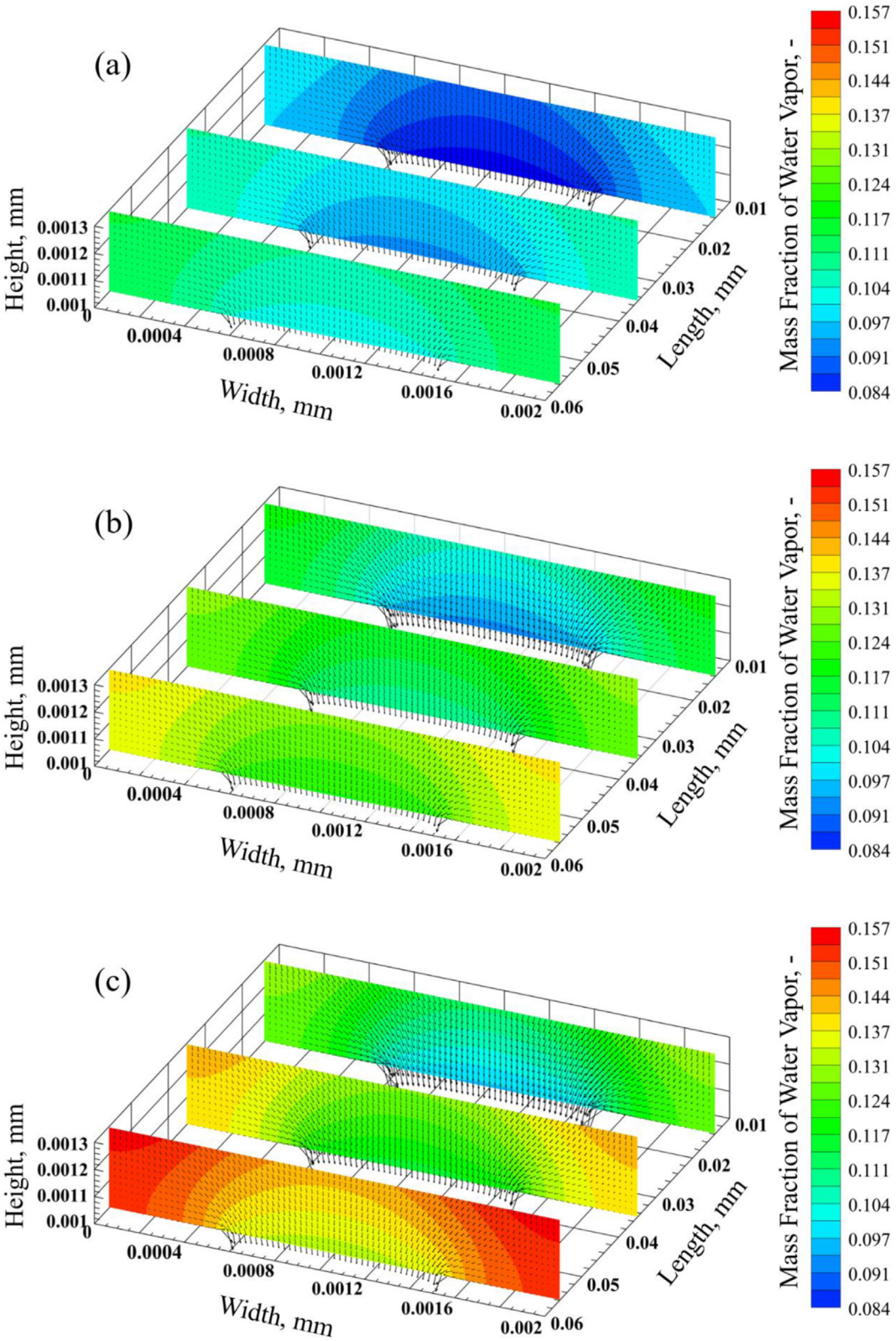

Fig. 6 – Schematic of vapor velocity distribution at different output voltages: (a) $V_{cell} = 0.7$ V, (b) $V_{cell} = 0.6$ V and (c) $V_{cell} = 0.5$ V.

Please cite this article as: Zhang M et al., Moisture migration in the cathode GDL of PEMFC under variable physical parameters based on a modified two-fluid model, International Journal of Hydrogen Energy, https://doi.org/10.1016/j.ijhydene.2023.01.055

higher condensation rate, so the liquid water saturation in the GDL becomes relatively higher, which will be explained in detail in the next section.

Migration of liquid water

Unlike the migration of water vapor, the transport of liquid water in GDL depends mainly on the driving effect of capillary pressure and the adhesion of the solid skeleton to liquid water [38]. According to the Leverett-J equation, the local capillary pressure in the GDL can be approximated by the water saturation at that location. For hydrophobic GDL, the higher the water saturation, the higher the capillary pressure, which drives the flow of liquid water from the highly saturated region to the less saturated region driven by the capillary pressure. The adhesion of the solid skeleton is defined as its dragging force to impede the movement of the liquid, And the Darcy's law considers both of these mechanisms. However, according to the continuous assumption, liquid water is also subject to the dragging effect of gas flow, the effect of phase change of water vapor, and its own inertia and viscosity. These mechanisms mentioned above are reflected in the momentum equation of the liquid phase, and the modified liquid water distribution is obtained through the solving of the modified model proposed in this paper.

The distribution of liquid water in the cathode GDL and its migration velocity are shown in Fig. 7. The selection of the reference cross-sections and the working conditions are consistent with Fig. 5. It can be seen that the distribution of liquid water is roughly similar to the distribution trend of water vapor, but the obstructing effect of the rib is more significant to the liquid water, leading to a uniform liquid water distribution along the Y-axis direction. This distribution determines that the velocity of liquid water in the GDL shows a tendency to discharge from the CL side to the runner side. It should be noted that the velocity of liquid water is several orders of magnitude smaller than the migration velocity of water vapor. For instance, under the 0.6 V working condition, the average discharge velocity of liquid water in the three cross-sections along the flow direction is 5.050×10^{-7}, 5.718×10^{-7}, and 6.396×10^{-7} m/s, respectively.

The three cross-sections under the same operating conditions show that the overall liquid water content in the GDL is also increased along the flow direction in the flow channel, which is mainly due to the increase in condensation rate along the flow direction. According to Fig. 6, it is known that the water vapor mass fraction in the GDL grows along the flow direction in the flow channel, which leads to the supersaturated vapor and therefore a gradual increase in the condensation rate. Unlike the vapor, the change in distance from the flow channel inlet has little effect on the velocity of liquid water discharging into the flow channel, which is resulted from the smaller capillary pressure gradient. As the current density increases, the increase in cathode water production causes the liquid water saturation in the GDL and the velocity of liquid water to increase, which results in a greater discharge of liquid water from the GDL into the channel at higher current densities. Microscopically, the increase in water saturation leads to a longer average distance between the gas-liquid interface and the solid skeleton surface inside the cell, and thus the solid skeleton is less able to bind water, which is the fundamental cause of more likely movement of liquid water in a high level of water saturation.

For the modified model proposed in this paper, all the effects except capillarity and viscosity of the solid skeleton are reduced to the correction factor $\vec{\delta}$. The three components of the factor are applied to the equations in three different directions, reflecting the deviation of the velocity calculated by Darcy's law from the real velocity, i.e., the influence of other neglected factors on the transport of liquid water. Fig. 8 shows the variation of this correction coefficient along the three directions, and the average value of the GDL cross-sections perpendicular to the corresponding direction is used as the basis of analysis.

In general, among the three components of the correction coefficients, δ_z is relatively larger, and in some regions the one is already close to 1 (in fact, the real value in some regions may be larger due to the fact that the factor is a surface average), while the magnitudes of δ_x and δ_y are relatively smaller, which means that the original Darcy model may have a larger error in describing the velocity component in the z-direction of liquid water. As can be seen in Fig. 8, due to the symmetry of the computational model, the distribution of the correction factors in the x-direction also shows symmetry, with the correction factors on the rib side being higher than those on the runner side; the correction factors in the y-direction show a decreasing trend from the channel side to the CL side; and the correction coefficients in the z-direction show a decreasing and then increasing trend along the flow direction in the channel. The primary reason for the above phenomena is that the velocity difference between liquid water and gas will produce drag force at the interface, which is not considered in Darcy's law. On the one hand, the viscous effect of rib on the liquid water is stronger than that on the gas, which will cause a stronger relative motion between the two phases, so the viscous sticking effect near the ribbed plate will be more obvious. On the other hand, due to the low saturation of liquid water, the calculated liquid velocity is also largely influenced by the change in water saturation. Compared to that of other positions, the smaller liquid water saturation at the entrance of the flow channel leads to a relatively small liquid water velocity and a larger velocity difference between the gas and liquid phases, thus having a larger drag force. And with the accumulation of liquid water, the liquid water saturation increases and the liquid film within the porous media is fully developed. Although the velocity difference is reduced, the average thickness of the liquid film is greater, the velocity is faster, and the inertia effect is more significant. The above two factors lead to a trend of correction factors shown in Fig. 8. It is worth mentioning that the phase transition rate is lower in this model, so the effect on the momentum change of the gas and liquid phases is lower compared to other factors.

It can be seen that in the calculation of the PEMFC with a single channel, the interaction between gas and liquid and the inertia of the liquid phase have certain effects on the transport of liquid water, which is more significant in areas such as near the rib and entrance of the channel. In terms of magnitude, the influence of these factors on the velocity in the z-direction

Please cite this article as: Zhang M et al., Moisture migration in the cathode GDL of PEMFC under variable physical parameters based on a modified two-fluid model, International Journal of Hydrogen Energy, https://doi.org/10.1016/j.ijhydene.2023.01.055

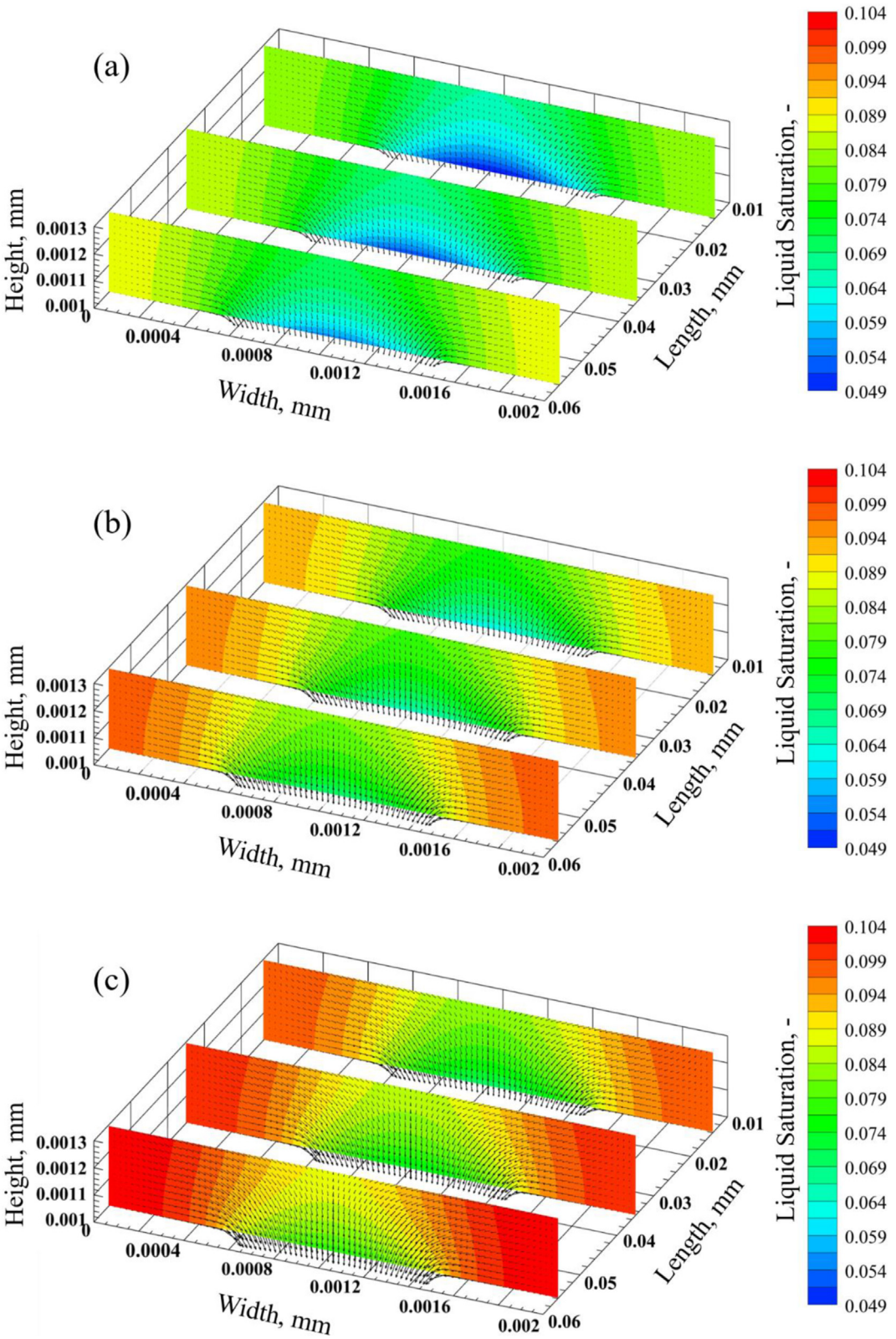

Fig. 7 – Schematic of liquid water velocity distribution at different output voltages: (a) $V_{cell} = 0.7$ V, (b) $V_{cell} = 0.6$ V and (c) $V_{cell} = 0.5$ V.

Please cite this article as: Zhang M et al., Moisture migration in the cathode GDL of PEMFC under variable physical parameters based on a modified two-fluid model, International Journal of Hydrogen Energy, https://doi.org/10.1016/j.ijhydene.2023.01.055

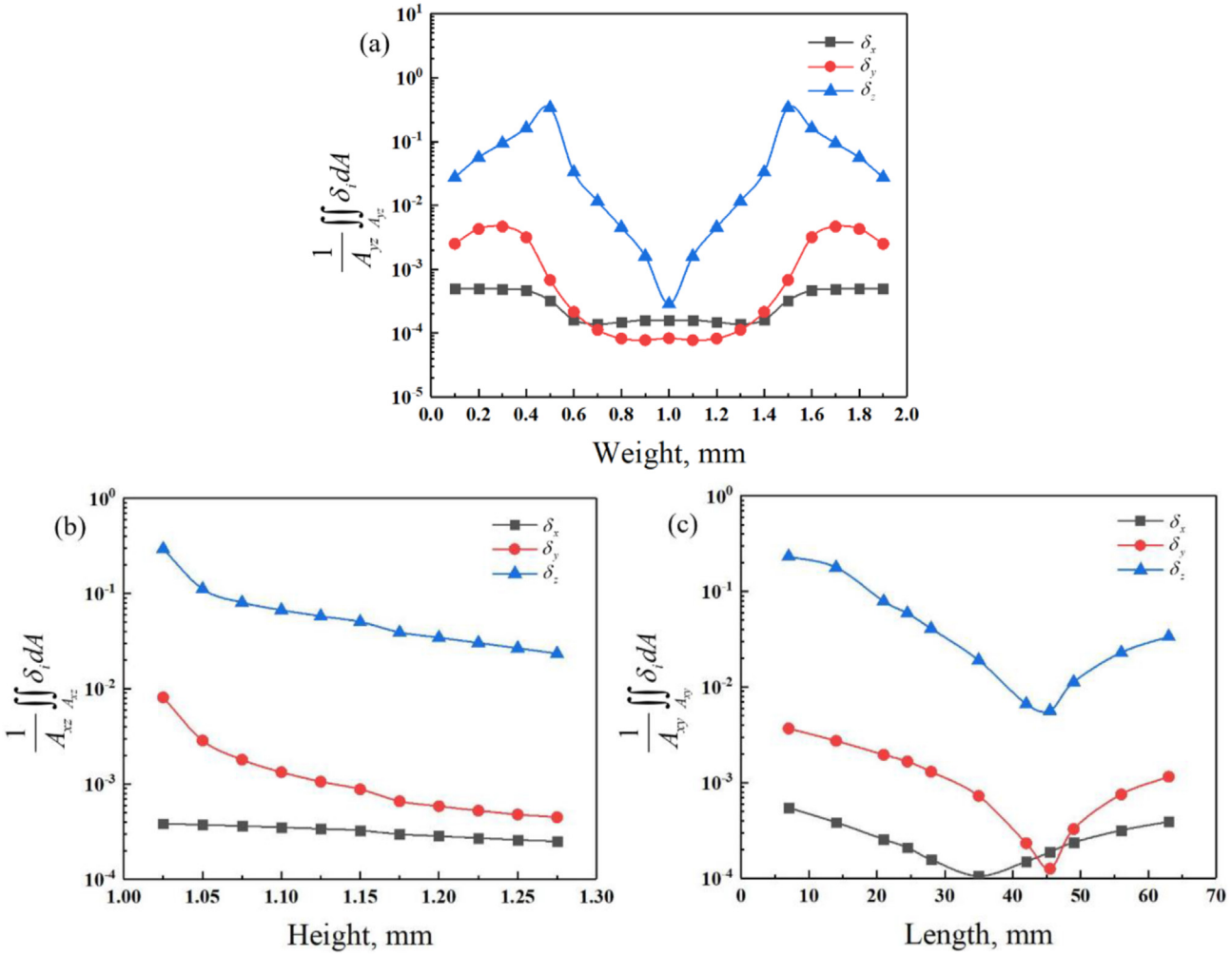

Fig. 8 – The area-weighted averages of different normal upward relative correction factors δ_i: (a) *x*-axis, (b) *y*-axis and (c) *z*-axis.

is greater compared to the other two directions, which means that the two-fluid model needs to be corrected while predicting the moisture migration and the distribution of the water saturation field changing along the flow channel direction even more. Therefore, for the simulation of multi-channel PEMFC stack with higher gas velocity and larger water saturation, the modified model has greater potential.

Impact of porosity

Porosity is an important parameter of GDL, and its value and distribution significantly affect the cell performance and the probability of flooding. The common values of porosity are about 0.2–0.8, and certain cases are selected in this study to investigate the effect of porosity in this range. It should be noted that since porosity can largely affect the permeability and thus have a complex effect on the calculation results, the permeability is fixed to be 1.76×10^{-11} m^2 in this calculation to investigate the effect of porosity alone. The trends of PEMFC current density and water saturation level in the cathode GDL for different porosity are shown in Fig. 9. In general, the higher the porosity, the lower the resistance of the GDL to reactants transport, and the more the corresponding intense chemical

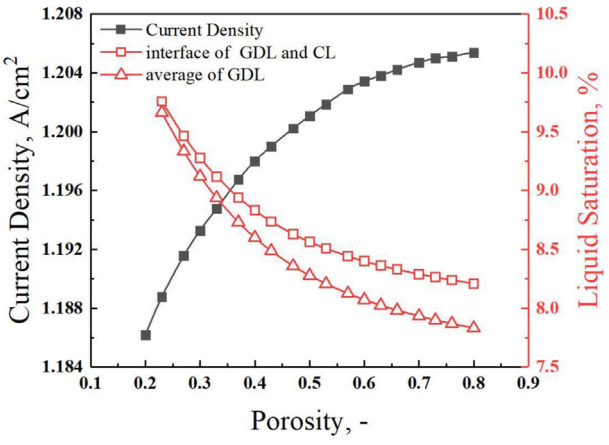

Fig. 9 – Variation of current density and water saturation in cathode porous media with different porosity at $V_{cell} = 0.6$ V and $K_{gdl} = 1.76 \times 10^{-11}$ m^2.

reactions, which leads to an improvement of the electrical performance of the cell. At the same time, larger porosity will also reduce the level of water saturation at the interface

Please cite this article as: Zhang M et al., Moisture migration in the cathode GDL of PEMFC under variable physical parameters based on a modified two-fluid model, International Journal of Hydrogen Energy, https://doi.org/10.1016/j.ijhydene.2023.01.055

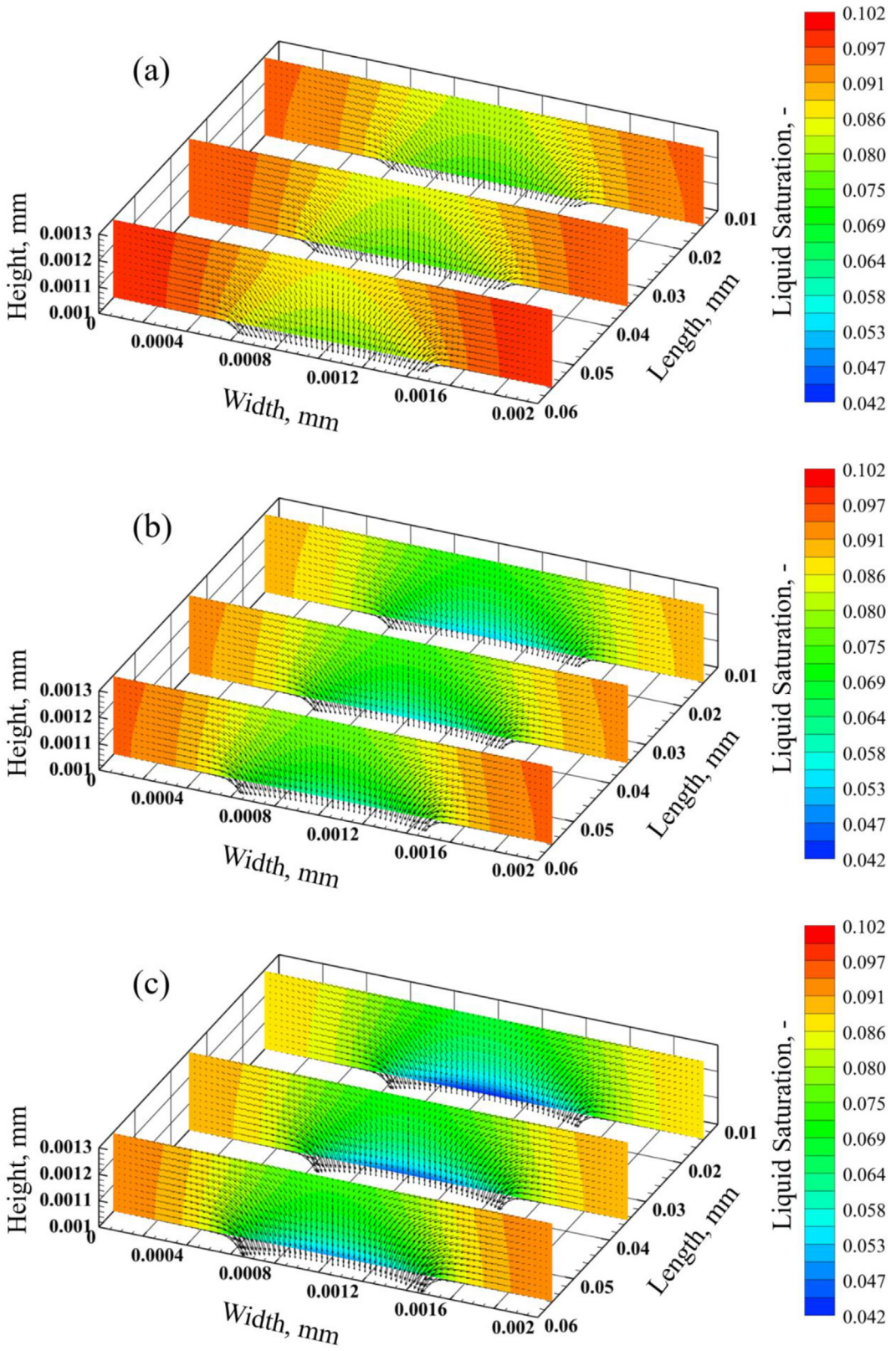

Fig. 10 – Schematic of liquid water velocity distribution with different porosity at $V_{cell} = 0.6$ V and $K_{gdl} = 1.76 \times 10^{-11}$ m^2: (a) $\varepsilon_{gdl} = 0.3$, (b) $\varepsilon_{gdl} = 0.5$ and (c) $\varepsilon_{gdl} = 0.7$.

Please cite this article as: Zhang M et al., Moisture migration in the cathode GDL of PEMFC under variable physical parameters based on a modified two-fluid model, International Journal of Hydrogen Energy, https://doi.org/10.1016/j.ijhydene.2023.01.055

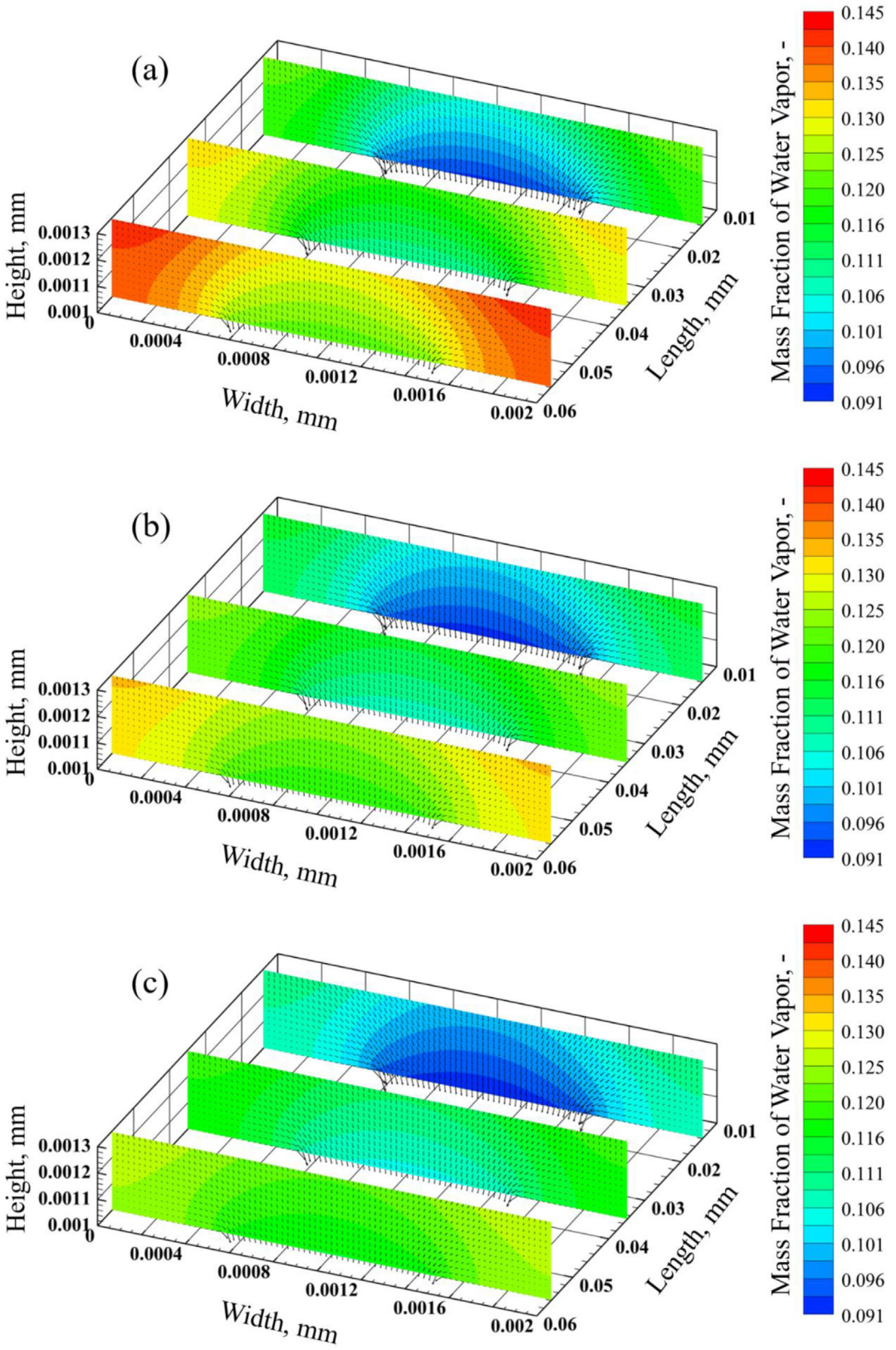

Fig. 11 – Schematic of vapor velocity distribution with different porosity at $V_{cell} = 0.6$ V and $K_{gdl} = 1.76 \times 10^{-11}$ m^2: (a) $\varepsilon_{gdl} = 0.3$, (b) $\varepsilon_{gdl} = 0.5$ and (c) $\varepsilon_{gdl} = 0.7$.

Please cite this article as: Zhang M et al., Moisture migration in the cathode GDL of PEMFC under variable physical parameters based on a modified two-fluid model, International Journal of Hydrogen Energy, https://doi.org/10.1016/j.ijhydene.2023.01.055

between GDL and CL, thus declining the risk of water flooding. On the other hand, an increase in porosity leads to a decrease in the solid phase share of the GDL and a consequent decrease in the electrical conductivity and physical pressure-bearing capacity. According to the trend shown in Fig. 9, the increase in porosity slows down the growth rate of PEMFC output current density due to the weakened conductivity. For GDL materials with low intrinsic conductivity, the output current density may instead decrease as the porosity increases [39].

Figs. 10 and 11 show the distributions of liquid and gaseous water velocity and content in the cathode GDL for three porosities of 0.3,0.5, and 0.7, respectively. It can be seen that the increase of porosity facilitates the discharge of both forms of water. Due to the increased porosity, the solid skeleton in the GDL becomes less, resulting in a reduced resistance to liquid water transport. What's more, the increase in porosity changes the capillary pressure gradient distribution in the GDL, and thus makes the liquid water more inclined to flow along the sidewalls of the channel, which is beneficial to the discharge of liquid water through the flow channel walls in a practical system [40]. For the gas phase, the increase in porosity also reduces the gas transport resistance and thus the distribution of gaseous components in the GDL becomes more uniform. In addition, the liquid water level in the GDL is lower for larger porosity away from the flow channel inlet, so it is more necessary to select larger porosity for GDL for electric stacks with longer flow channel distribution such as serpentine flow channels.

Impact of permeability

Permeability is an important parameter describing the resistance to material transport in unsaturated porous media, and its value depends on the material of the porous media, porosity, pore tortuosity, etc., and ranges from 10^{-10}-10^{-14} m^2 in common studies. In previous studies, the effect of permeability on the performance of PEMFC was considered to be insensitive [35]. However, in fact, the value of permeability has a very important impact on the liquid phase transport capacity of PEMFC, thus affecting the probability of cell flooding. A decrease in permeability will, on the one hand, increase the capillary pressure gradient in the GDL and enhance the drive force for mass transfer, and on the other hand, increase the mass transfer resistance in the GDL and hinder the liquid water transport therein.

In this paper, the electrical performance of the cell and the water saturation in the cathode GDL under different permeability were investigated with reference to previous experimental data, and the results are shown in Fig. 12. It can be seen that at permeability lower than about 1.4×10^{-11} m^2, lower permeability leads to lower current density and higher level of water saturation at the GDL and CL interface, which can block the transport of reactants into CL. While, when the permeability is greater than 1.4×10^{-11} m^2, the increase in permeability shows an opposite but slight phenomenon.

The trend of current density is exactly opposite to the trend of water saturation at the GDL and CL interface, so it can be deduced that the effect of permeability on the electrical performance of the cell comes from the blockage of the GDL pores

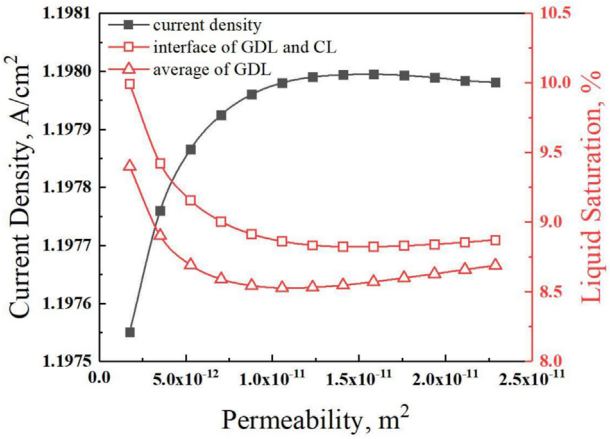

Fig. 12 – Variation of current density and water saturation in cathode porous media with different permeability at $V_{cell} = 0.6$ V and $\varepsilon_{gdl} = 0.4$.

by liquid water, which is further supported by the liquid water distribution and transport diagram shown in Fig. 13. According to Fig. 13(a), at lower permeability (1.760×10^{-12} m^2), even with a higher capillary pressure gradient as the driving force, the liquid water discharge capacity is still poor due to the large interphase resistance for the liquid water transport, which results in a high water saturation at the GDL and CL interface and hinders the transport of oxygen to the electrochemical reaction site. After the permeability exceeds the critical permeability of 1.408×10^{-11} m^2, the interphase resistance decays gradually at a slower rate due to the inverse relationship between the magnitude of transport resistance and permeability. At this moment, the weakening effect of the lower capillary pressure gradient on transport becomes more significant, so that the liquid water in the porous media layer appears slightly elevated at the higher permeability (2.288×10^{-11} m^2) level. Therefore, there should be a relatively optimal value for the selection of GDL with different permeability that can maximize the efficiency of liquid water discharge.

The effect of permeability on gaseous water transport is mainly reflected in the gas-liquid interphase resistance, and this value is relatively small compared to the pressure drive force, so the effect of permeability changes on gaseous water transport is not significant. In the range of permeability studied in this paper, the transport of gaseous water is basically consistent with that shown in Fig. 6(b).

Conclusion

In the present study, a 3D multiphase flow model of PEMFCs is developed to investigate the migration characteristics of water in the cathode GDL of the cell under steady-state operating conditions based on the assumption of unsaturated porous media and REV method. To solve the model, the velocity of liquid and vapor were obtained according to the diffusion equation and the liquid water momentum equation, respectively. The effects of porosity and permeability on the cell performance and material transport are also investigated.

Please cite this article as: Zhang M et al., Moisture migration in the cathode GDL of PEMFC under variable physical parameters based on a modified two-fluid model, International Journal of Hydrogen Energy, https://doi.org/10.1016/j.ijhydene.2023.01.055

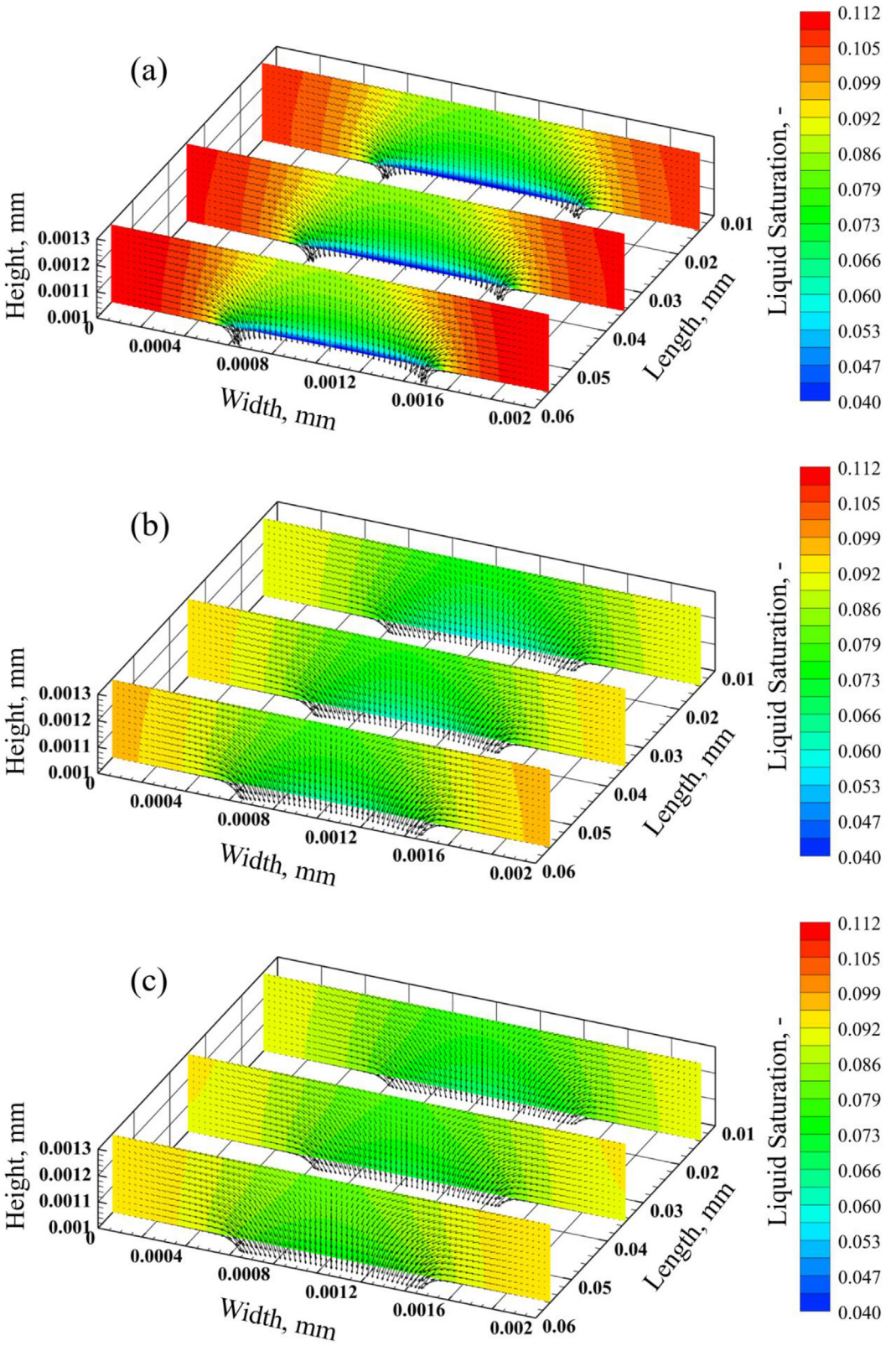

Fig. 13 – Schematic of liquid water velocity distribution with different permeability at $V_{cell} = 0.6$ V and $\varepsilon_{gdl} = 0.4$: (a) $K_{gdl} = 0.176 \times 10^{-11}$ m^2, (b) $K_{gdl} = 1.408 \times 10^{-11}$ m^2 and (c) $K_{gdl} = 2.288 \times 10^{-11}$ m^2.

Please cite this article as: Zhang M et al., Moisture migration in the cathode GDL of PEMFC under variable physical parameters based on a modified two-fluid model, International Journal of Hydrogen Energy, https://doi.org/10.1016/j.ijhydene.2023.01.055

Based on the derivations and investigations the following conclusions can be obtained.

(1) In the cathode GDL of PEMFC, both water vapor and liquid water show a tendency to be transported from the internal CL to the external channel, and the water distribution trends of both forms are generally similar. The presence of the ribs affects the pressure and capillary pressure distribution inside the GDL, which makes the transport velocity of moisture near the rib side relatively larger. For this study, the discharge velocity of liquid water is several orders of magnitude smaller than that of water vapor (about 10^{-7} m/s for liquid water and 10^{-3} m/s for water vapor), so the water vapor is the main discharge form of the moisture from the GDL, which accounted for more than 90% of discharged water study.
(2) The influence of porosity on the performance parameters of PEMFC lies in the electrical conductivity of the skeleton and the transport capacity of both gas and liquid. As the porosity increases, on the one hand, the weaker confinement of the solid skeleton for liquid water makes the free water component increased, thus making the liquid water to discharge more fluent, and the water saturation at the intersection of CL and GDL is significantly reduced, which is conducive to the entry of oxygen into CL. On the other hand, the growth of current density of PEMFC will be suppressed or even reduced due to the reduced volume share of solid skeleton, and the conductivity of GDL will be weakened accordingly. As far as the electrical and mechanical properties allow, the highest possible porosity is helpful for cell performance and preventing flooding.
(3) The influence of permeability on PEMFC performance parameters mainly lies in the transport of liquid water. For the same porosity and output voltage, there exists a relatively good threshold value of permeability (about 1.5×10^{-11} m^2 for this model). When the permeability is higher than this threshold, the decrease of capillary pressure gradient weakens the liquid water drainage in GDL. And when the permeability is below this value, the increase in permeability causes the resistance term of liquid water to increase significantly and thus the liquid water discharge capacity is limited. Even though the electrical performance of the cell is not sensitive to changes in permeability, the distribution of liquid water inside the GDL prominently depends on the magnitude of the permeability. There exists a relatively optimal value of permeability (about 1.5 × 10–11 m^2 for this work) that can preferably prevent flooding of the cathode GDL.

Declaration of competing interest

The authors declare that they have no known competing financial interests or personal relationships that could have appeared to influence the work reported in this paper.

Acknowledgements

This work was supported by the National Natural Science Foundation of China (No. 52076096), the Natural Science Foundation of Hubei Province (No. 2020CFA040) and Wuhan Applied Foundational Frontier Project (No. 2020010601012205).

REFERENCES

[1] Sharaf OZ, Orhan MF. An overview of fuel cell technology: fundamentals and applications. Renew Sustain Energy Rev 2014;32:810–53. https://doi.org/10.1016/j.rser.2014.01.012.
[2] Wang Y, Ruiz Diaz DF, Chen KS, et al. Materials, technological status, and fundamentals of PEM fuel cells – a review. Mater Today 2020;32:178–203. https://doi.org/10.1016/j.mattod.2019.06.005.
[3] Pei H, Liu Z, Zhang H, et al. In situ measurement of temperature distribution in proton exchange membrane fuel cell I a hydrogen–air stack. J Power Sources 2013;227:72–9. https://doi.org/10.1016/j.jpowsour.2012.11.027.
[4] Jiao K, Li X. Water transport in polymer electrolyte membrane fuel cells. Prog Energ Combust 2011;37:221–91. https://doi.org/10.1016/j.pecs.2010.06.002.
[5] Litster S, Sinton D, Djilali N. Ex situ visualization of liquid water transport in PEM fuel cell gas diffusion layers. J Power Sources 2006;154:95–105. https://doi.org/10.1016/j.jpowsour.2005.03.199.
[6] Chen L, Wang Y-F, Tao W-Q. Experimental study on the effect of temperature and water content on the thermal conductivity of gas diffusion layers in proton exchange membrane fuel cell. Therm Sci Eng Prog 2020;19:100616. https://doi.org/10.1016/j.tsep.2020.100616.
[7] Chen G, Zhang G, Guo L, et al. Systematic study on the functions and mechanisms of micro porous layer on water transport in proton exchange membrane fuel cells. Int J Hydrogen Energy 2016;41:5063–73. https://doi.org/10.1016/j.ijhydene.2016.01.074.
[8] Bazylak A. Liquid water visualization in PEM fuel cells: a review. Int J Hydrogen Energy 2009;34:3845–57. https://doi.org/10.1016/j.ijhydene.2009.02.084.
[9] Zhang G, Jiao K. Multi-phase models for water and thermal management of proton exchange membrane fuel cell: a review. J Power Sources 2018;391:120–33. https://doi.org/10.1016/j.jpowsour.2018.04.071.
[10] Springer TE, Zawodzinski TA, Gottesfeld S. Polymer electrolyte fuel cell model. J Electrochem Soc 1991;138:2334–42. https://doi.org/10.1149/1.2085971.
[11] Bernardi DM, Verbrugge MW. A mathematical model of the solid-polymer-electrolyte fuel cell. J Electrochem Soc 1992;139:2477–91. https://doi.org/10.1149/1.2221251.
[12] Nguyen TV, White RE. A water and heat management model for proton-exchange-membrane fuel cells. J Electrochem Soc 1993;140:2178–86. https://doi.org/10.1149/1.2220792.
[13] Fuller TF, Newman J. Water and thermal management in solid-polymer-electrolyte fuel cells. J Electrochem Soc 1993;140:1218–25. https://doi.org/10.1149/1.2220960.
[14] Singh D, Lu DM, Djilali N. A two-dimensional analysis of mass transport in proton exchange membrane fuel cells. Int J Eng Sci 1999;37:431–52. https://doi.org/10.1016/S0020-7225(98)00079-2.
[15] Um S, Wang C-Y, Chen KS. Computational fluid dynamics modeling of proton exchange membrane fuel cells. J Electrochem Soc 2000;147:4485–93. https://doi.org/10.1149/1.1394090.

Please cite this article as: Zhang M et al., Moisture migration in the cathode GDL of PEMFC under variable physical parameters based on a modified two-fluid model, International Journal of Hydrogen Energy, https://doi.org/10.1016/j.ijhydene.2023.01.055

[16] Berning T, Lu DM, Djilali N. Three-dimensional computational analysis of transport phenomena in a PEM fuel cell. J Power Sources 2002;106:284–94. https://doi.org/10.1016/S0378-7753(01)01057-6.
[17] Berning T, Djilali N. A 3D, multiphase, multicomponent model of the cathode and anode of a PEM fuel cell. J Electrochem Soc 2003;150:A1589–98. https://doi.org/10.1149/1.1621412.
[18] Meng H. A two-phase non-isothermal mixed-domain PEM fuel cell model and its application to two-dimensional simulations. J Power Sources 2007;168:218–28. https://doi.org/10.1016/j.jpowsour.2007.03.012.
[19] Adroher XC, Wang Y. Ex situ and modeling study of two-phase flow in a single channel of polymer electrolyte membrane fuel cells. J Power Sources 2011;196:9544–51. https://doi.org/10.1016/j.jpowsour.2011.07.076.
[20] Havaej P, Kermani MJ, Abdollahzadeh M, et al. A numerical modeling study on the influence of catalyst loading distribution on the performance of Polymer Electrolyte Membrane Fuel Cell. Int J Hydrogen Energy 2018;43:10031–47. https://doi.org/10.1016/j.ijhydene.2018.04.063.
[21] Zhang G, Jiao K. Three-dimensional multi-phase simulation of PEMFC at high current density utilizing Eulerian-Eulerian model and two-fluid model. Energy Convers Manag 2018;176:409–21. https://doi.org/10.1016/j.enconman.2018.09.031.
[22] Wang ZH, Wang C-Y, Chen KS. Two-phase flow and transport in the air cathode of proton exchange membrane fuel cells. J Power Sources 2001;94:40–50. https://doi.org/10.1016/S0378-7753(00)00662-5.
[23] You LX, Liu HT. A two-phase flow and transport model for the cathode of PEM fuel cells. Int J Heat Mass Tran 2002;45:2277–87. https://doi.org/10.1016/S0017-9310(01)00322-2.
[24] Wang Y. Modeling of two-phase transport in the diffusion media of polymer electrolyte fuel cells. J Power Sources 2008;185:261–71. https://doi.org/10.1016/j.jpowsour.2008.07.007.
[25] Sun P. A Dirichlet/Robin iteration-by-subdomain method for an anisotropic, nonisothermal two-phase transport model of PEM fuel cell with micro-porous layer. J Comput Appl Math 2014;270:241–56. https://doi.org/10.1016/j.cam.2014.01.014.
[26] Hao L, Cheng P. Lattice Boltzmann simulations of anisotropic permeabilities in carbon paper gas diffusion layers. J Power Sources 2009;186:104–14. https://doi.org/10.1016/j.jpowsour.2008.09.086.
[27] Chen L, Xiang X, Wang S, et al. Effects of Pt particle on structure and protons transport of Nafion membrane. Int J Heat Mass Tran 2020;148:118977. https://doi.org/10.1016/j.ijheatmasstransfer.2019.118977.
[28] Anderson R, Zhang L, Ding Y, et al. A critical review of two-phase flow in gas flow channels of proton exchange membrane fuel cells. J Power Sources 2010;195:4531–53. https://doi.org/10.1016/j.jpowsour.2009.12.123.
[29] Liu W, Peng SW, Mizukami K. Moisture evaporation and migration in thin porous packed bed influenced by ambient and operating conditions. Int J Energy Res 1997;21:41–53. https://doi.org/10.1002/(SICI)1099–114X. 199701)21:1<41::AID-ER246>3.0.CO;2-Z.
[30] Son J, Um S, Kim Y-B. Numerical analysis of the effect of anisotropic gas diffusion layer permeability on polymer electrolyte membrane fuel cell performance with various channel types. Fuel 2021;289:119888. https://doi.org/10.1016/j.fuel.2020.119888.
[31] Qiu D, Janßen H, Peng L, et al. Electrical resistance and microstructure of typical gas diffusion layers for proton exchange membrane fuel cell under compression. Appl Energy 2018;231:127–37. https://doi.org/10.1016/j.apenergy.2018.09.117.
[32] Liu W, Peng SW, Mizukami K. A general mathematical modelling for heat and mass transfer in unsaturated porous media: an application to free evaporative cooling. Heat Mass Tran 1995;31:49–55. https://doi.org/10.1007/BF02537421.
[33] Liu W, Zhao XX, Mizukami K. 2D numerical simulation for simultaneous heat, water and gas migration in soil bed under different environmental conditions. Heat Mass Tran 1998;34:307–16. https://doi.org/10.1007/s002310050264.
[34] Chen H, Guo H, Ye F, et al. A numerical study on convection and diffusion of mass transfer in proton exchange membrane fuel cells with orientated-type flow channels. Int J Energy Res 2020;45:5659–78. https://doi.org/10.1002/er.6191.
[35] Tao WQ, Min CH, Liu XL, et al. Parameter sensitivity examination and discussion of PEM fuel cell simulation model validation. J Power Sources 2006;160:359–73. https://doi.org/10.1016/j.jpowsour.2006.01.078.
[36] Wang L. A parametric study of PEM fuel cell performances. Int J Hydrogen Energy 2003;28:1263–72. https://doi.org/10.1016/s0360-3199(02)00284-7.
[37] Afshari E. Computational analysis of heat transfer in a PEM fuel cell with metal foam as a flow field. J Therm Anal Calorim 2019;139:2423–34. https://doi.org/10.1007/s10973-019-08354-x.
[38] Nam JH, Kaviany M. Effective diffusivity and water-saturation distribution in single- and two-layer PEMFC diffusion medium. Int J Heat Mass Tran 2003;46:4595–611. https://doi.org/10.1016/s0017-9310(03)00305-3.
[39] Xia L, Ni M, He Q, et al. Optimization of gas diffusion layer in high temperature PEMFC with the focuses on thickness and porosity. Appl Energy 2021:300. https://doi.org/10.1016/j.apenergy.2021.117357.
[40] Zhang FY, Yang XG, Wang C-Y. Liquid water removal from a polymer electrolyte fuel cell. J Electrochem Soc 2006;153:A225–32. https://doi.org/10.1149/1.2138675.

Please cite this article as: Zhang M et al., Moisture migration in the cathode GDL of PEMFC under variable physical parameters based on a modified two-fluid model, International Journal of Hydrogen Energy, https://doi.org/10.1016/j.ijhydene.2023.01.055